Al-Rafidain Engineering Journal (AREJ) Vol.31, No.3, September 2026, pp. 72-83

LR-Aided Linear Detection Combined with Adaptive QRD-M in MIMO-OFDM Systems

Mar Mar Lwin* **Mohd Fadzli Mohd Salleh*** **Salah Abdulghani Alabady****
mar.mar.lwin@student.usm.my fadzlisalleh@usm.my eng.salah@uomosul.edu.iq

* School of Electrical and Electronic Engineering, Universiti Sains Malaysia, Seri Ampangan, 14300, Nibong Tebal, Pulau Pinang, Malaysia
**Computer Engineering Department, College of Engineering, University of Mosul, Mosul, Iraq

Received: October 7th 2025 Received in revised form: March 4th 2026 Accepted: March 14th 2026

ABSTRACT

This paper proposes an LR-aided adaptive QRD-M detector for complexity reduction in MIMO-OFDM systems. The proposed approach integrates lattice-reduction preprocessing with an adaptive candidate selection strategy to control the search width of the QRD-M algorithm. Unlike the conventional QRD-M detector with a fixed candidate size, the proposed method dynamically adjusts the number of surviving paths to limit unnecessary computations while preserving detection reliability. Simulation results demonstrate that the proposed detector achieves near-optimal detection performance in frequency-selective MIMO-OFDM channels, reaching a symbol error rate (SER) of 10^{-5} for an 8×8 system using 16-QAM modulation at high SNR. For a 4×4 configuration, the proposed method reduces computational complexity by approximately 26% in terms of average squared Euclidean distance (SED) computations compared with the conventional QRD-M detector. Analytical FLOP evaluation further confirms consistent complexity savings as the antenna dimension increases. These results demonstrate an improved performance–complexity trade-off and strong scalability for practical large-scale MIMO deployments.

Keywords:

MIMO systems, Detection methods, LLL lattice reduction, QRD-M, Spatial Multiplexing.

https://rengj.uomosul.edu.iq/index.php/rengj/index
Email: alrafidain_engjournal3@uomosul.edu.iq

===

1. INTRODUCTION

Multiple-input multiple-output orthogonal frequency-division multiplexing (MIMO-OFDM) is a key technology in modern wireless communication systems due to its high spectral efficiency and robustness against multipath fading. However, reliable signal detection in MIMO-OFDM systems remains computationally challenging, especially for large antenna configurations and high-order modulation schemes, motivating the development of efficient near-optimal detection algorithms.

Maximum-likelihood (ML) detection achieves optimal error-rate performance but requires exhaustive search with exponential complexity, making it impractical for real-time MIMO-OFDM systems [1], [2]. Linear detectors, such as zero-forcing (ZF) and minimum mean-square error (MMSE), significantly reduce computational complexity but suffer from noise enhancement and residual inter-stream interference in ill-conditioned channels [2]. To balance performance and complexity, tree-search-based detectors have been widely investigated. Sphere decoding provides near-ML performance but exhibits highly variable complexity [2], [3] fixed-complexity detectors, such as the K-best and QRD-M algorithms, limit the number of surviving paths per layer to achieve predictable complexity [4], [5]. Recent studies have further refined tree-search-based detection strategies. An adaptive Dijkstra-based tree search detector was introduced by [6] in which node expansion is regulated via path-metric comparisons to control complexity. A layer-prioritized detection scheme tailored for 5G RedCap user equipment under high-order modulation was reported by [7]. A permutation-based breadth-first search algorithm was proposed by [8] to reduce computational complexity and latency through varied detection orderings and early termination mechanisms. A sort-free Box Decoding approach was presented by [9], employing deterministic pruning rules to regulate candidate expansion while maintaining near-K-best performance. To further improve detection reliability, preprocessing techniques based on QR decomposition and lattice reduction have been employed to enhance channel orthogonality and reduce noise amplification before tree search [10], [11].

Despite these advances, conventional QRD-M detection relies on a fixed number of surviving paths, resulting in inefficient path exploration across varying channel and noise conditions. The path-elimination QRD-M scheme proposed by [12] reduces computational complexity by pruning unlikely branches using accumulated squared Euclidean distance metrics, while preserving near-ML detection performance in MIMO-OFDM systems. However, the pruning process requires repeated metric comparisons and threshold checks at each detection stage, which increases the decision logic and limits scalability as the system scales. The upper–lower bounded-complexity QRD-M algorithm proposed by [13] achieves substantial complexity reduction by bounding the search using a Babai-distance-based criterion. Still, its pruning behaviour is governed by predefined bounds rather than fully adapting to instantaneous layer-wise reliability.

This motivates the need for a QRD-M-based detection approach that adaptively controls the search process based on instantaneous channel conditions, while maintaining near-ML performance with reduced computational complexity.

The paper is organized as follows: Section 2 provides an overview of the system model fundamentals; Section 3 presents the proposed LR-Aided Adaptive QRD-M Algorithm; Section 4 analyzes the computational complexity; Section 5 presents the results and their corresponding discussions; Section 6 concludes the paper.

2. THE THEORETICAL BASES

A MIMO system with N_T transmitting and N_R receiving antennas, where $N_R \geq N_T$, is considered. The received signal y is given by [14].

$$\boldsymbol{y} = \mathbf{H}\boldsymbol{x} + \boldsymbol{n} \quad (1)$$

where the transmit vector $\boldsymbol{x} = \begin{bmatrix} x_1 \\ x_2 \\ \vdots \\ x_{N_T} \end{bmatrix}$,

the received signal vector $\boldsymbol{y} = \begin{bmatrix} y_1 \\ y_2 \\ \vdots \\ y_{N_R} \end{bmatrix}$,

the noise vector $\boldsymbol{n} = \begin{bmatrix} n_1 \\ n_2 \\ \vdots \\ n_{N_R} \end{bmatrix}$,

and the channel matrix

$$\mathbf{H} = \begin{bmatrix} h_{11} & h_{12} & \dots & h_{1N_T} \\ h_{21} & h_{22} & \dots & h_{2N_T} \\ \vdots & \vdots & \ddots & \vdots \\ h_{N_R1} & h_{N_R2} & \dots & h_{N_RN_T} \end{bmatrix}.$$

Each element h_{ij} in the channel matrix, the propagation coefficient between the j-th transmitting antenna and the i-th receiving antenna. These coefficients are modeled as independent, identically distributed (i.i.d.) complex Gaussian random variables with a mean of zero and a variance of one ($\sigma_n^2 = 1$). As a result, the channel matrix $\mathbf{H}$ is of size $N_R \times N_T$ and has a rank of N_T, characterizing a Rayleigh flat-fading scenario. In this model, the receiver has complete knowledge of the channel state information (CSI), whereas the transmitter operates without access to it. The transmitted signal $\boldsymbol{x}$ can be estimated using the Integer Least Squares (ILS) equation.

$$\hat{\boldsymbol{x}}_{ML} = \arg \min_{\boldsymbol{x} \in \mathbb{C}^{N_T}} \|\boldsymbol{y} - \mathbf{H}\boldsymbol{x}\|^2 \quad (2)$$

where $\mathbb{C}$ denotes the complex signal constellation (eg., QAM), and $\mathbb{C}^{N_T}$ presents all possible set of transmit symbol vectors across the N_T to the transmit antennas. The estimate $\hat{\boldsymbol{x}}_{ML}$ denotes the most likely transmitted signal, determined by minimizing the Euclidean distance between the received signal $\boldsymbol{y}$ and the reconstructed symbol $\mathbf{H}\boldsymbol{x}$.

The complexity of solving Eq. (2) is NP-hard and exponential. The matrix $\mathbf{H}$ is initially transformed orthogonally via a QR decomposition into a reduced upper-triangular matrix. Thus, the right-hand side of (2) becomes:

$$\begin{aligned} \|\boldsymbol{y} - \mathbf{H}\boldsymbol{x}\|^2 &= \|\boldsymbol{y} - \mathbf{QR}\boldsymbol{x}\|^2 \\ &= \|\boldsymbol{y}\mathbf{Q}^H - \mathbf{Q}^H\mathbf{QR}\boldsymbol{x}\|^2 \\ &= \|\hat{\boldsymbol{y}} - \mathbf{R}\boldsymbol{x}\|^2 \end{aligned}$$

where $\hat{\boldsymbol{y}} = \boldsymbol{y}\mathbf{Q}^H$.

Also, Eq. (2) becomes:

$$\hat{\boldsymbol{x}} = \arg \min_{\boldsymbol{x} \in \mathbb{C}^{N_T}} \|\hat{\boldsymbol{y}} - \mathbf{R}\boldsymbol{x}\|^2 \quad (3)$$

For example, $N_T = N_R = 4$, $\|\hat{\boldsymbol{y}} - \mathbf{R}\boldsymbol{x}\|^2$ may be expanded as:

$$\left\| \begin{bmatrix} \hat{y}_1 \\ \hat{y}_2 \\ \hat{y}_3 \\ \hat{y}_4 \end{bmatrix} - \begin{bmatrix} R_{11} & R_{12} & R_{13} & R_{14} \\ 0 & R_{22} & R_{23} & R_{24} \\ 0 & 0 & R_{33} & R_{34} \\ 0 & 0 & 0 & R_{44} \end{bmatrix} \begin{bmatrix} x_1 \\ x_2 \\ x_3 \\ x_4 \end{bmatrix} \right\|^2 \quad (4)$$

And the Squared Euclidean Distance (SED) of Eq. (4) is calculated as:

$$\begin{gathered} SED = \|\hat{y}_4 - R_{44}\, x_4\|^2 \\ +\|\hat{y}_3 - R_{33}\, x_3 - R_{34}\, x_4\|^2 \\ +\|\hat{y}_2 - R_{22}\, x_2 - R_{23}\, x_3 - R_{24}\, x_4\|^2 \\ +\|\hat{y}_1 - R_{11}\, x_1 - R_{12}\, x_2 - R_{13}\, x_3 - \\ R_{14}\, x_4\|^2 \end{gathered}$$

In general, the above expansion is expressed as,

$$\|\hat{\boldsymbol{y}} - \mathbf{R}\boldsymbol{x}\|^2 = \sum_{i=1}^{N_T} \left\| \hat{y}_i - \sum_{j=i}^{N_T} R_{ij} x_j \right\|^2 \quad (5)$$

The element R_{ij} represents the entry located at the i-th row and j-th column of matrix **R**. Similarly, $\hat{y}_i$ corresponds to the i-th received signal, while x_j denotes the transmitted signal from the j-th antenna. This work considers a scenario in which the number of transmit and receive antennas is the same. Fig. 1 illustrates the tree structure of conventional QRD-M detection with fixed M, where candidate symbol branches are pruned based on the SED at each detection layer.

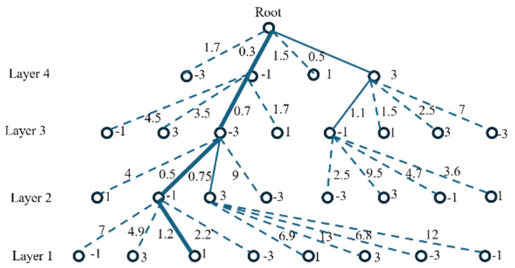

Fig. 1 Tree structure of conventional QRD-M detection with fixed M

Fig. 1 illustrates the tree-search process of conventional QRD-M detection with a fixed candidate size M. Starting from the root node at the highest detection layer after QR decomposition, each surviving node is expanded by appending all possible symbol candidates at the current layer. The squared Euclidean distance (SED) is computed for each candidate, and only the Mpaths with the smallest SED values are retained, while the remaining paths are pruned. This breadth-first pruning procedure is repeated layer by layer until the final detection layer, where the transmitted symbol vector is determined.

3. THE PROPOSED LR-AIDED ADAPTIVE QRD-M ALGORITHM

Fig. 2 illustrates the overall system block diagram of the proposed adaptive QRD-M detection scheme integrated within the MIMO receiver.

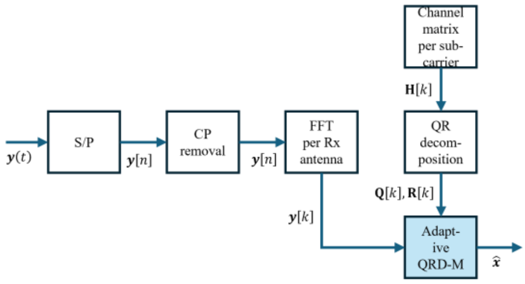

Fig. 2 System block diagram of the proposed LR-aided adaptive QRD-M detection

As shown in Fig. 2, the received baseband signals at the multiple antennas are processed by the MIMO-OFDM front end, including serial-to-parallel conversion, cyclic prefix removal, and FFT, producing frequency-domain observations. For each subcarrier, the $N_R \times N_T$ MIMO channel is treated as a narrowband flat-fading system and decomposed via QR, yielding orthonormal **Q** and upper-triangular **R** matrices. These matrices are then used by the proposed adaptive QRD-M detector, which performs layer-wise tree-search symbol estimation to generate the transmit symbol vector.

In conventional QRD-M detection, symbol estimation is performed using a breadth-first tree search (BFTS) starting from the N_T-th detection layer after QR decomposition. At each layer, all constellation symbols are considered as candidates, and the squared Euclidean distance (SED) is used as the branch metric. Only a fixed number $M$of candidate paths with the smallest metrics are retained at each layer.

At the $N_T{}^{\text{th}}$ layer, the branch metric corresponding to the l-th constellation symbol c_l is given by

$$E_{N_T}^{l} = \left|\hat{y}_{N_T} - R_{N_T N_T}\ c^{l}\right|^2 \quad (6)$$

where l = 1, 2, …., L.

All L branch metrics are sorted in ascending order, and the Msymbols with the smallest SED values are selected as surviving parent nodes for the next layer.

At the $(N_T\!-\!1)$-th layer, each surviving parent node is expanded by appending all Lconstellation symbols, resulting in $M \times L$candidate paths. The corresponding branch metrics are computed as

$$E_{N_T-1}^{l} = \left|\hat{y}_{N_T-1} - \left(R_{N_T-1N_T-1}c_l + R_{N_T-1N_T}\hat{x}_{N_T,m}\right)\right|^2 \quad (7)$$

where $m = 1,2,\dots,M$ denotes the surviving candidates from the previous layer. This process continues recursively toward the first layer, and the general branch metric at the i-th layer is expressed as

$$E_i^{(l)} = \sum_{i=1}^{N_T} \left\| \hat{y}_i - R_{ii}c_l - \sum_{j=i+1}^{N_T} R_{ij}\,\hat{x}_{j,m} \right\|^2 \quad (8)$$

A. LR-Based Threshold Derivation

To enable adaptive pruning, lattice reduction (LR) is applied to the channel matrix using the LLL algorithm, yielding a reduced basis $\tilde{\mathbf{H}} = \mathbf{HT}$, where $\mathbf{T}$ is a unimodular matrix. The system model is transformed as

$$\boldsymbol{y} = \mathbf{H}\boldsymbol{x} + \boldsymbol{n} = \tilde{\mathbf{H}}\boldsymbol{s} + \boldsymbol{n} \quad (9)$$

Performing QR decomposition on $\tilde{\mathbf{H}}$ gives

$$\tilde{\mathbf{H}} = \tilde{\mathbf{Q}}\,\tilde{\mathbf{R}} \quad (10)$$

where $\tilde{\mathbf{Q}}$ is a unitary matrix and $\tilde{\mathbf{R}}$ is an upper-triangular matrix.
Multiplying both sides of (9) by $\tilde{\mathbf{Q}}^H$ gives

$$\tilde{\mathbf{Q}}^H\boldsymbol{y} = \tilde{\mathbf{Q}}^H\tilde{\mathbf{Q}}\,\tilde{\mathbf{R}}\boldsymbol{s} + \tilde{\mathbf{Q}}^H\boldsymbol{n} \quad (11)$$

Since $\tilde{\mathbf{Q}}^H\tilde{\mathbf{Q}} = \mathbf{I}$, define: $\hat{\boldsymbol{y}} = \tilde{\mathbf{Q}}^H\boldsymbol{y}$, $\hat{\boldsymbol{n}} = \tilde{\mathbf{Q}}^H\boldsymbol{n}$ leading to

$$\hat{\boldsymbol{y}} = \tilde{\mathbf{R}}\boldsymbol{s} + \hat{\boldsymbol{n}} \quad (12)$$

Based on the LR-reduced system, a Babai estimate of the symbol at the N_Tth detection layer is obtained as

$$\hat{s}_{N_T} = \mathcal{Q}\left(\frac{\hat{y}_{N_T}}{\tilde{R}_{N_TN_T}}\right) \quad (13)$$

where $\mathcal{Q}(\cdot)$ denotes the quantization operation, the corresponding SED is used to define the pruning threshold.

$$\eta_{N_T} = \left|\hat{y}_{N_T} - \hat{s}_{N_T}\right|^2 \quad (14)$$

The threshold for the root layer, η_{N_T}, is derived based on the Babai point and lattice reduction principles, providing a reference value for evaluating candidate paths in the MIMO detection process.

B. Adaptive Pruning and M Updating

For the i-th detection layer, the threshold is generalized as η_i. Candidate paths whose branch metrics exceed this threshold are discarded. The surviving paths determine the updated value of M for the next layer. Paths are sorted in ascending order of their branch metrics, and pruning continues sequentially until the threshold is exceeded, allowing the algorithm to adjust complexity based on channel conditions adaptively.

By combining LR-based thresholding with breadth-first tree search, redundant paths are eliminated early in the detection process, reducing the number of metric computations.

C. Design Choice: Branch-Metric-Based Evaluation

Unlike prior work that relies on accumulated path metrics, the proposed method uses individual branch metrics to guide pruning. This design assumes that the most reliable detection paths originate from parent nodes with smaller branch metrics. By evaluating metrics at each branching step rather than along the entire path, the approach significantly reduces computational complexity while maintaining near-ML detection performance.

4. COMPLEXITY ANALYSIS

Computational complexity can be expressed in various ways, including execution time (e.g., latency or CPU time) or closed-form representations such as Big-O notation. In this paper, complexity is evaluated using two complementary metrics: the number of floating-point operations (FLOPs) required to estimate the transmitted vector $\boldsymbol{x}$, and the number of squared Euclidean distance (SED) computations as a function of SNR. This dual evaluation provides a comprehensive assessment of computational burden and algorithmic efficiency.

The conventional QRD-M maintains a fixed number of candidate paths at each detection layer, resulting in a predictable computational load determined by N_T, the predefined number of surviving candidates M, and the modulation order. In contrast, the proposed adaptive QRD-M adjusts the number of surviving candidates based on the pruning criterion, resulting in SNR-dependent computational behavior. For consistency, the complexity of both approaches is evaluated using FLOP counts and SED computations.

Table 1 summarizes the computational requirements of key arithmetic operations in terms of real multiplications and additions: ADD represents real addition, MUL denotes real multiplication, ADDc refers to complex addition, and MULc indicates complex multiplication. Throughout this paper, a real multiplication, division, or square root is counted as 1 FLOP, while a real addition counts as 0.5 FLOP. Using these conventions, the complexity of the conventional QRD-M and the proposed LR-aided adaptive QRD-M detection methods is determined and compared.

Table 1**:** Computation of arithmetic operations

Operation	Inputs	Output	Complexity	Flops
Complex addition	Both complex	Complex	2ADD	1.0
Complex multiplication	Both complex	Complex	4MUL +2ADD	5.0
Multiplication (Complex by real)	Complex and real	Complex	2MUL	2.0
Square root	Real	Real	1MUL	1.0
Complex power	Complex	Real	2MUL +1ADD	2.5
Real division	Both real	Real	1MUL	1.0
Complex division	Both complex	Complex	8MUL +3ADD	9.5
Complex division (Complex by real)	Complex and real	Complex	2MUL	2.0

The inversion of a square matrix with dimensions $[N_T \times N_T]$ requires N_T^3 multiplication operations and N_T^3 addition operations [15]. The number of floating-point operations (FLOPs) needed for matrix inversion, as outlined in Table 1, is $6N_T^3$.

Consider the matrix multiplication involving a matrix Q^H of dimension $N_R \times N_R$ and a received signal vector y of dimension $N_R \times 1$. According to the principles of matrix multiplication, this process requires $N_R(N_R - 1)$ addition operations and N_R^2 multiplication operations. The number of floating-point operations (FLOPs) required for $Q^H y$, as presented in Table 1, is $3N_R^2 - N_R$.

The number of floating-point operations (FLOPs) required to perform QR decomposition is approximately $2N_T^3$ [15], [16].

Therefore, the number of floating-point operations (FLOPs) required to perform QR decomposition, matrix inversion, and $\mathbf{Q}^H \boldsymbol{y}$ is:

$$8N_T^3 + 3N_R^2 - N_R \tag{15}$$

The above computational complexity calculations are comparable to those of tree-search-based detection methods. However, in Sphere Decoding (SD), the branch metric computation for all constellation points within the sphere radius is particularly intensive, making it more complex than QRD-M detection. Specifically, the total number of branch metrics that need to be calculated in QRD-M detection is:

$$N_B = L + \sum_{i=1}^{N_T-1} L \times M \tag{16}$$

where L is the number of constellations and M is the design value.

Therefore, using Table 1, the number of flops, F, to calculate the Euclidean Distances becomes:

$$F = 8.5L + \sum_{n=2}^{N_T} 6nML + 2.5ML \tag{17}$$

The sum of integers from 1 to N is given by:

$$\sum_{i=1}^{N} i = \frac{N(N+1)}{2} = \frac{N^2}{2} + \frac{N}{2} \tag{18-a}$$

So, the sum of integers from 2 to N is:

$$\sum_{i=2}^{N} i = \left(\frac{N(N+1)}{2}\right) - 1 = \frac{N^2}{2} + \frac{N}{2} - 1 \tag{18-b}$$

will be utilized to (16) and becomes:

$$F = 8.5L + 2.5ML + 6ML\left(\frac{{N_T}^2}{2} + \frac{N_T}{2} - 1\right) \tag{19}$$

The number of flops required for comparison is 0.5 L flops for N_T-th layer and 0.5ML flops for $(N_T - 1)$-th layer.

So, the number of FLOPs, F, required to calculate conventional QRD-M is given as:

$$F_{QRD-M} = 8N_T^3 + 3N_R^2 - N_R + 9L + 3ML + 6ML\left(\frac{{N_T}^2}{2} + \frac{N_T}{2} - 1\right) \tag{20}$$

When $N_T = N_R = N$ and the complexity of QRD-M detection in flops is:

$$F_{QRD-M} = 8N^3 + (3ML+3)N^2 + (3ML-1)N - 3ML + 9L \quad (21)$$

The computational complexity of the proposed LR-aided adaptive QRD-M method is evaluated by varying the design parameter M and accounting for the LLL algorithm's complexity. Generally, the proposed LR-aided adaptive QRD-M exhibits lower complexity compared to the conventional QRD-M. This reduction is attributed to the selected M value in the proposed LR-aided adaptive QRD-M being consistently smaller than in the traditional approach, resulting in fewer branch metric computations.

The complexity of the LLL algorithm is analysed here for 8×8 MIMO, with a maximum of 6 iterations.

- The size reduction requires $(N_{max} - 2) \times \{1 \times (Div) + 2 \times (Mult + Add)\} = 16$ FLOPs
- The Lovàsz condition requires $\{4 \times (Mult) + 2 \times (Add)\} = 5$ FLOPs
- The Givens rotation matrix computation requires $\{2 \times (Div) + 2 \times (Mult) + 1 \times (Add) + 1 \times (Sqrt)\} = 6.5$ FLOPs
- The rotation operation for R (matrix multiplication) requires $2 \times \{2 \times (Mult) + 1 \times (Add)\} \times N_R = 5N$ FLOPs
- The rotation operation for Q (matrix multiplication) requires $2 \times \{2 \times (Mult) + 1 \times (Add)\} \times 2 = 12$ FLOPs
- The flag condition sum requires $N_T(Add) = 0.5\,N$ FLOPs

So, the total number of flops for the LLL algorithm, assuming a maximum iteration of 6, is

$$F_{LLL} = 16 + 5 + 6.5 + 5N + 12 + 0.5N = 39.5 + 6N \text{ FLOPs} \quad (22)$$

It is evident that LLL complexity is lower than branch metric calculation, which is $\mathcal{O}(N^3)$. Therefore, the number of flops to compute the proposed system is:

$$F_{proposed} = 8N^3 + \left(3M_{avg}L + 3\right)N^2 + \left(3M_{avg}L - 1\right)N - 3M_{avg}L + 9L + 39.5 + 6N \quad (23)$$

where M_{avg} is the average value of M from $N_T{}^{\text{th}}$ layer to the first layer.

In this case, the complexity is solely determined by the quantity M of design values. When compared to M calculations, lattice reduction's complexity is insignificant. The M_{avg}, design M value is always less than the value in conventional QRD-M. The proposed LR-aided adaptive QRD-M algorithm achieves low complexity by pruning unlikely candidate paths, thereby reducing the number of branch metric calculations.

5. RESULTS AND DISCUSSION

This section evaluates the symbol error rate (SER) performance and computational complexity of the proposed LR-aided adaptive QRD-M detector. The proposed method is compared with Sphere Decoding (SD) and conventional QRD-M detection to demonstrate its effectiveness in achieving a favorable performance–complexity trade-off.

Table 2: Simulation parameters used for performance and complexity evaluation

Parameter	Value
FFT size (number of subcarriers)	64
OFDM symbols per frame	14 (for Monte Carlo averaging)
Cyclic prefix length	$N_{\text{FFT}}/4$
Channel model	Rayleigh flat fading (1-tap i.i.d.) and frequency-selective fading (N_{tap}= 5)
Number of channel taps	5
Power delay profile	Exponential
Modulation scheme	16-QAM, 64-QAM
MIMO configuration	4×4, 8×8
Detection methods	Conventional QRD-M, Proposed LR-aided adaptive QRD-M
Monte Carlo trials	1000

Table 2 indicates the required simulation parameters. Simulations are carried out using Monte Carlo trials for 4×4 and 8×8 MIMO configurations under Rayleigh flat-fading and frequency-selective fading channels. Both 16-QAM and 64-QAM modulation schemes are considered to assess scalability with respect to modulation order. For OFDM-based simulations, the FFT size is set to 64 with a cyclic prefix length of Nfft/4. The SNR range varies from 0 to 25 dB. The initial and minimum candidate sizes are set to M_{init} and M_{min}, respectively.

Figure 3 illustrates the SER performance of Sphere Decoding (SD) [17] and conventional

QRD-M with $M = 8, 12,$ and 16 for a 4×4 MIMO system employing 16-QAM modulation. As expected, SD provides the best performance and serves as the near-ML benchmark. For the QRD-M detector, increasing M improves SER performance, with $M = 16$ achieving performance closest to SD.

However, this improvement is obtained at the expense of increased computational complexity, since a larger M results in more retained candidate paths at each detection layer. These results highlight the inherent performance–complexity trade-off of conventional QRD-M detection and motivate the need for adaptive strategies that dynamically regulate the candidate set size.

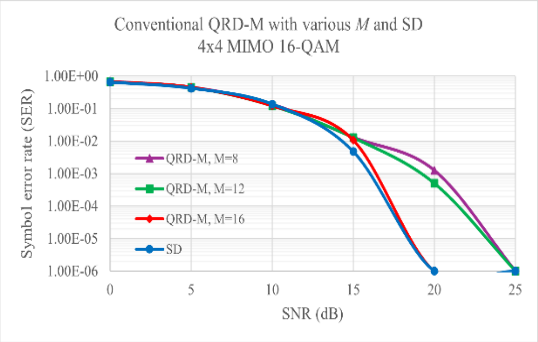

Fig. 3 Performance analysis of Sphere Decoding [17] and conventional QRD-M with M = 8, 12, and 16 in a 4×4 MIMO system using 16-QAM modulation scheme

Fig. 4 presents the SER performance of the proposed LR-aided adaptive QRD-M detector compared with conventional QRD-M using different fixed values of M in a 4×4 MIMO system with 16-QAM modulation. The proposed detector achieves performance comparable to conventional QRD-M in the low-SNR region. In the medium-SNR range, its SER closely follows that of QRD-M with moderate M values (e.g., $M = 8$ and $M = 12$). At higher SNR levels, a performance gap is observed relative to QRD-M with larger fixed M; however, the proposed method maintains acceptable detection performance while avoiding the consistently high computational load associated with large M.

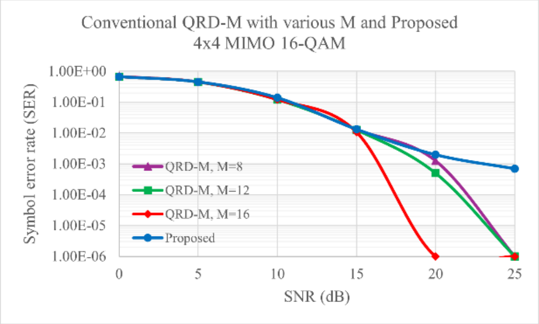

Fig. 4 Symbol error rate (SER) performance of the proposed LR-aided adaptive QRD-M and conventional QRD-M with various M for 4×4 MIMO 16-QAM modulation

Fig. 5 shows the average number of squared Euclidean distance (SED) computations versus SNR for the proposed LR-aided adaptive QRD-M and conventional QRD-M detectors in a 4×4 MIMO system with 16-QAM modulation. As expected, the conventional QRD-M exhibits constant complexity across the SNR range for each fixed value of M. In contrast, the proposed detector maintains a relatively stable computational load while operating below the complexity of larger fixed-M configurations (e.g., $M = 12$ and $M = 16$). This demonstrates that the adaptive pruning mechanism effectively controls the number of retained paths without incurring the consistently high complexity associated with large fixed M.

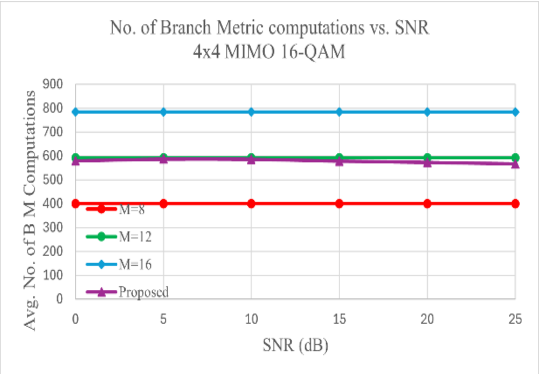

Fig. 5 Average number of squared Euclidean distance (SED) computations versus SNR for the proposed LR-aided adaptive QRD-M and conventional QRD-M for 4×4 MIMO 16-QAM modulation

Fig. 6 shows the SER performance of the proposed LR-aided adaptive QRD-M detector versus SNR for 16-QAM in 4×4 and 8×8 MIMO systems. In both configurations, the SER decreases steadily as SNR increases, demonstrating consistent detection performance under improved channel conditions.

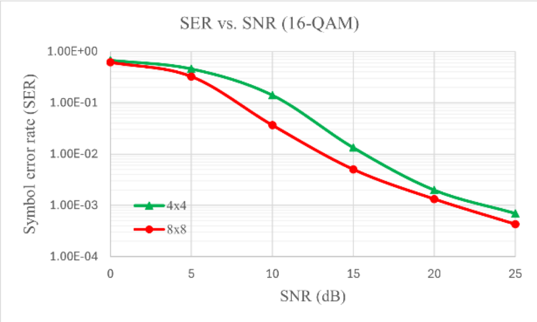

Fig. 6 Symbol error rate (SER) performance of the proposed LR-aided adaptive QRD-M detector for 4 × 4 and 8 × 8 MIMO systems using 16-QAM modulation

Fig. 7 presents the average number of branch metric (BM) computations versus SNR for the proposed LR-aided adaptive QRD-M detector with 16-QAM in 4 × 4 and 8 × 8 MIMO systems. For both configurations, only minor variations in BM count are observed across the SNR range, indicating that the pruning mechanism does not lead to a pronounced reduction in complexity at higher SNR under the considered simulation settings.

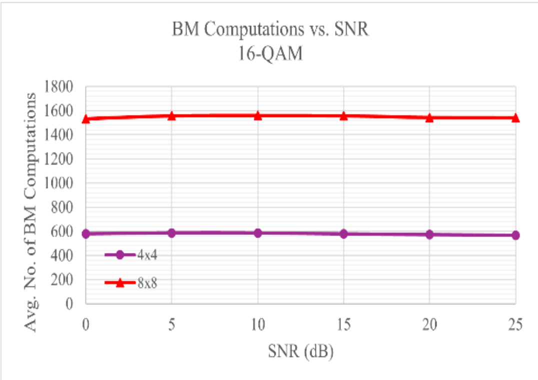

Fig. 7 Average number of squared Euclidean distance (SED) computations versus SNR for the proposed LR-aided adaptive QRD-M for 4 × 4 and 8 × 8 MIMO systems using 16-QAM modulation

To evaluate the detector under more practical channel conditions, a frequency-selective Rayleigh fading channel with five taps is considered within the MIMO-OFDM framework. The cyclic prefix is assumed sufficient to eliminate inter-symbol interference, allowing each subcarrier to be modeled as an equivalent flat MIMO channel in the frequency domain. Based on this setup, the SER performance of the proposed LR-aided adaptive QRD-M detector is examined for 4 × 4 and 8 × 8 antenna configurations using 16-QAM modulation. As shown in Fig. 8, the SER decreases monotonically with increasing SNR for both configurations. The 8 × 8 system achieves consistently lower error rates than the 4 × 4 case, indicating that the proposed detector effectively leverages the increased spatial diversity while maintaining stable performance under multipath fading conditions.

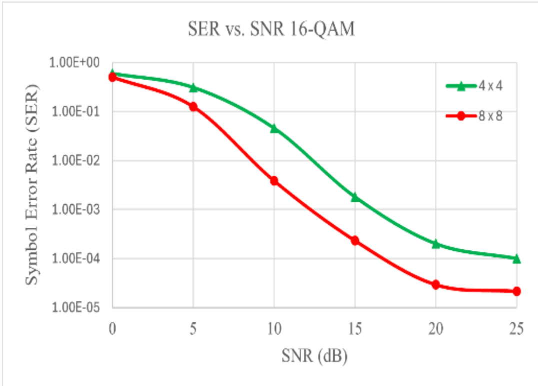

Fig. 8 Symbol error rate (SER) performance for 4 × 4 and 8 × 8 MIMO-OFDM, 16-QAM modulation,frequency-selective channel, 5 taps

Fig. 9 illustrates the average number of squared Euclidean distance (SED) computations versus SNR for the proposed LR-aided adaptive QRD-M detector under the frequency-selective MIMO-OFDM scenario. The SED count exhibits only minor variations across the SNR range for both 4 × 4 and 8 × 8 configurations, indicating that the pruning strategy effectively bounds the search effort and ensures a predictable computational load. Although the 8 × 8 system incurs higher complexity due to its larger dimensionality, the overall behavior confirms controlled candidate expansion under multipath channel conditions.

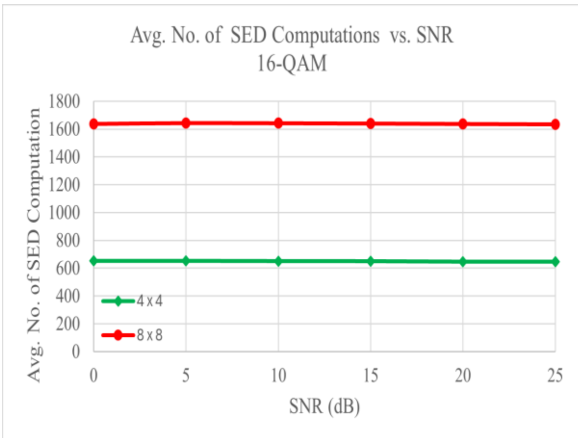

Fig. 9 Average number of squared Euclidean distance (SED) computations versus SNR (4×4

and 8×8 MIMO-OFDM, 16-QAM modulation) under a frequency-selective channel, 5 taps

In addition to the SED-based evaluation, analytical complexity is assessed using floating-point operation (FLOP) expressions that explicitly account for arithmetic operations. The conventional QRD-M detector is evaluated with a fixed candidate size equal to the constellation size. In contrast, the proposed detector employs a derived FLOP model based on the average candidate width obtained from simulation. As the analysis is based on the detector processing structure rather than runtime measurements, a consistent hardware-independent comparison is ensured.

Fig. 10 compares the analytical FLOP requirements of the conventional QRD-M and the proposed detector as the number of transmit antennas increases. The computational cost of both detectors grows with the system dimension; however, the proposed detector consistently requires fewer FLOPs than the conventional QRD-M due to its reduced average candidate width. The gap between the two curves becomes more pronounced as antenna dimensions increase, indicating improved computational efficiency in high-dimensional MIMO systems. These results confirm that the proposed approach achieves tangible complexity savings while preserving the underlying QRD-M processing structure.

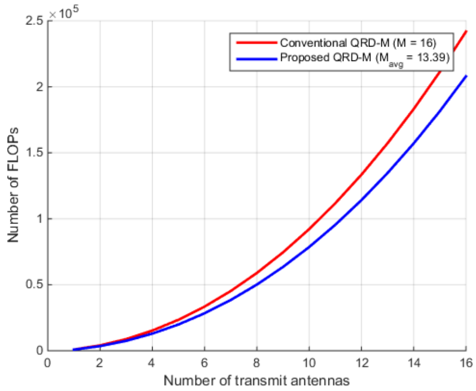

Fig. 10 FLOP comparison between the conventional QRD-M and the proposed detector

To further illustrate the overall efficiency of the proposed detector, Table 3 summarizes the performance–complexity trade-off between the conventional QRD-M and the proposed method. By jointly considering SER performance and computational cost, the table highlights that the proposed detector achieves comparable error performance while requiring fewer computational resources. This confirms that the complexity reduction observed in both SED and FLOP evaluations does not come at the expense of detection reliability.

Table 3 Performance–complexity trade-off of the proposed LR-aided adaptive QRD-M detector compared with the conventional QRD-M detector

SNR [dB]	MIMO configuration	Modulation	Complexity (Conventional QRD-M)	Complexity (Proposed LR-Aided adaptive QRD-M)	SER (Conventional QRD-M)	SER (Proposed LR-Aided adaptive QRD-M)
10	4 × 4	16-QAM	784	586	0.1213	0.1405
15	4 × 4	16-QAM	784	578	0.01067	0.01332
25	4 × 4	16-QAM	784	566	0	0.0006992
10	8 × 8	16-QAM	1808	1560	0.1588	0.03654
15	8 × 8	16-QAM	1808	1557	0.00075	0.00502
25	8 × 8	16-QAM	1808	1540	0	0.0004297

6. CONCLUSION

This paper presented an LR-aided adaptive QRD-M detector for complexity reduction in MIMO-OFDM systems. Simulation results for a 4×4 MIMO-OFDM system with 16-QAM modulation demonstrate that the proposed method achieves SER performance comparable to that of the conventional QRD-M detector while reducing average SED computations by approximately 26%. Analytical FLOP evaluation further confirms consistent complexity savings as the antenna dimension increases. The proposed detector therefore provides an improved performance–complexity trade-off and exhibits strong scalability for larger MIMO configurations.

ACKNOWLEDGEMENTS

The authors thank the School of Electrical and Electronic Engineering, Universiti Sains Malaysia, for providing the academic environment that facilitated this research.

REFERENCES

[1] S. Kumar, P. Tiwari, and M. Zymbler, "Internet of Things is a revolutionary approach for future technology enhancement: a review," *J. Big Data*, vol. 6, no. 1, Dec. 2019, doi: 10.1186/s40537-019-0268-2.

[2] S. Yang and L. Hanzo, "Fifty Years of MIMO Detection: The Road to Large-Scale MIMOs," *IEEE Communications Surveys & Tutorials*, Jul. 2015, doi: 10.1109/COMST.2015.2475242.

[3] Agrell, Eriksson, and Vardy, "Chalmers Publication Library Copyright Notice," 2002. [Online]. Available: http://www.ieee.org/documents/opsmanual.pdf

[4] Z. Guo and P. Nilsson, "Algorithm and implementation of the K-best Sphere decoding for MIMO detection," *IEEE Journal on Selected Areas in Communications*, vol. 24, no. 3, pp. 491–503, Mar. 2006, doi: 10.1109/JSAC.2005.862402.

[5] W. H. Chin, "QRD based tree search data detection for MIMO communication systems," in *2005 IEEE 61st Vehicular Technology Conference*, 2005, pp. 1624–1627.

[6] K. Boukari, "Adaptive Dijkstra's Search Algorithm for MIMO detection 9 Original Scientific Papers," Feb. 2022. doi: https://doi.org/10.32985/ijeces.13.1.2.

[7] Xin Wang, Xu Zhao, Jie Gan, Xinggen Qu, Jiang Shao, and Baozhi Zhang, "Research on MIMO Detection Method for 5G Redcap UE with High Order Modulation," in *International Conference on Internet of Things, Communication and Intelligent Technology*, Singapore: Springer, Apr. 2024, pp. 212–223.

[8] Y. Tian, W. Bian, J. Zheng, W. Zhou, Y. Huang, and C. Zhang, "Breadth-First Search Detection With Permutation Channel for Massive MIMO," *IEEE Wireless Communications Letters*, vol. 14, no. 9, pp. 2678–2682, 2025, doi: 10.1109/LWC.2025.3575277.

[9] S. Yang, A. S. Bora, E. Matus, and G. Fettweis, "Box Decoding with Low-Complexity Sort-free Candidate Pruning for MIMO Detection," Nov. 2025, [Online]. Available: http://arxiv.org/abs/2512.00653

[10] W. Dirk, B. Ronald, and K. Volker, "Near-Maximum-Likelihood Detection of MIMO Systems using MMSE-Based Lattice-Reduction," *communications, 2004 IEEE international Conference*, vol. 2, no. c, pp. 798–802, 2004, doi: 10.1109/ICC.2004.1312611.

[11] D. Wubben, D. Seethaler, J. Jalden, and G. Matz, "Lattice reduction," *IEEE Signal Process. Mag.*, vol. 28, no. 3, pp. 70–91, May 2011, doi: 10.1109/MSP.2010.938758.

[12] J. H. Ro, J. K. Kim, Y. H. You, and H. K. Song, "Low-complexity QRD-M with path eliminations in MIMO-OFDM systems," *Applied Sciences (Switzerland)*, vol. 7, no. 12, Nov. 2017, doi: 10.3390/app7121206.

[13] M. Mohaisen and K. Chang, "Upper-Lower Bounded-Complexity QRD-M for Spatial Multiplexing MIMO-OFDM Systems," May 2010. doi: 10.1007/s11277-010-0014-8. pp. 129-141

[14] T.-D. Chiueh, P. Tsai, and I.-W. Lai, *Baseband receiver design for wireless MIMO-OFDM communications*, Second Edition. John Wiley & Sons Singapore Pte. Ltd., 2012.

[15] S. U. Gene H. Golub and C. U. Charles F. Van Loan, *Matrix Computations*, 4th ed. Johns Hopkins University Press, 2013.

[16] W. K. Nicholson, "LINEAR ALGEBRA with Applications Open Edition BASE TEXTBOOK ADAPTABLE | ACCESSIBLE | AFFORDABLE Creative Commons License (CC BY-NC-SA)," 2019.

[17] A. Ghasemmehdi and E. Agrell, "Faster recursions in sphere decoding," *IEEE Trans. Inf. Theory*, vol. 57, no. 6, pp. 3530–3536, Jun. 2011, doi: 10.1109/TIT.2011.2143830.

Algorithm 1: The Proposed LR-Aided Adaptive QRD-M Algorithm

Input: H, y, PAM_table, M_min.

Output: estimated symbol vector $\hat{x}$

$[\mathrm{Q}, \mathrm{R}] \leftarrow qr(\mathrm{H})$ //QR decomposition for detection

$\hat{y} \leftarrow \mathrm{Q}^{H} y$ //Transformed received vector for metric computation

$[\widetilde{\mathrm{Q}}, \widetilde{\mathrm{R}}, \mathrm{T}] \leftarrow LLL(\mathrm{H})$ //Complex LLL for threshold computation

$\tilde{\mathrm{y}} \leftarrow \widetilde{\mathrm{Q}}\, y$ //Transformed received vector for threshold computation

// **Step 1**: Root layer (layer N_T)

for each symbol x in PAM_table **do**

  Initialize candidate branches at the N_T-th detection layer.

  $E_{N_T} \leftarrow \left|\hat{y}_{N_T} - R_{N_T,N_T} x\right|^2$ //Compute squared Euclidean distance

  $\hat{s}_{N_T} \leftarrow round\left(\frac{\tilde{y}_{N_T}}{\widetilde{\mathrm{R}}_{N_T,N_T}}\right)$ //Babai estimate

  $\eta_{N_T} \leftarrow \left|\hat{y}_{N_T} - \hat{s}_{N_T}\right|^2$ //Threshold

  if $E_{N_T} \leq \eta_{N_T}$ **then**

    Retain the candidate branches

  end if

end for

$M \leftarrow$ number of retained candidate branches

if $M < M\_min$ **then**

  $M \leftarrow M + 1$

end if

Store the top M surviving candidates for extension at the next layer

// **Step 2**: Remaining layers (from $N_T - 1$ to 1)

for layer $i = N_T - 1$ down to 1 **do**

  for each surviving branch, extend it with each symbol $x_i \in$ PAM_table **do**

    $contribution\_from\_lower\_layers \leftarrow \sum_{j=i+1}^{N_T} R_{i,j}\hat{x}_j$

    $E_i \leftarrow \left|\hat{y}_i - R_{i,i}x - contribution\_from\_lower\_layers\right|^2$

$babai\_term \leftarrow \sum_{j=i+1}^{N_T} \tilde{R}_{i,j}\, \hat{x}_j$

$\hat{s}_i \leftarrow round\big((\hat{y}_i - babai\_term)/\tilde{R}_{i,i}\big)$

$\eta_i \leftarrow |\hat{y}_i - \hat{s}_i|^2$ //Threshold

if $E_i \leq \eta_i$ **then**

Retain the candidate branches

end if

end for

$M \leftarrow$ number of retained candidate branches

if $M < M\_min$ **then**

$M \leftarrow M + 1$

end if

Store the top M surviving candidates for extension at the next layer

end for

// **Step 3**: Final decision

At layer 1, Select the surviving candidate with the minimum distance.

Reconstruct the full symbol vector $\hat{x}$ from the selected path

Return $\hat{x}$

End